Many-Photon Dynamics of Photobleaching

ARTICLE *in* THE JOURNAL OF PHYSICAL CHEMISTRY A · DECEMBER 2007

Impact Factor: 2.69 · DOI: 10.1021/jp074756x · Source: PubMed

6 AUTHORS, INCLUDING:

Sergey Polyutov
Siberian Federal University
20 PUBLICATIONS **138** CITATIONS
SEE PROFILE

Prakash Chandra Jha
KTH Royal Institute of Technology
33 PUBLICATIONS **252** CITATIONS
SEE PROFILE

Hans Agren
KTH Royal Institute of Technology
866 PUBLICATIONS **18,654** CITATIONS
SEE PROFILE

Many-Photon Dynamics of Photobleaching

S. Gavrilyuk,* S. Polyutov,† P. C. Jha, Z. Rinkevicius, H. Ågren, and F. Gel'mukhanov

Theoretical Chemistry, Royal Institute of Technology, Roslagstullsbacken 15, S-106 91 Stockholm, Sweden

Received: June 19, 2007; In Final Form: August 23, 2007

A detailed dynamical theory of photobleaching by periodical sequences of laser pulses is presented. The theory is used for interpretation of recent experiments with pyrylium salts. Our simulations are based on first-principles simulations of photoabsorption cross-sections and on empirical rate constants. Two competitive channels of photobleaching, namely, photobleaching from the lowest excited singlet and triplet states and from higher excited states, are found to explain different intensity dependences of the photobleaching rates in different samples. The process includes two-photon excitation from the ground state to the first or second excited singlet states and one-photon excitation from the first singlet or triplet states to higher excited states. The fluorescence follows double-exponential dynamics with two characteristic times. The first and the shorter one is the equilibrium settling time between the ground and the lowest triplet states. The second characteristic time, the time of photobleaching, is responsible for the long-term dynamics. The effective rate of photobleaching from the first excited singlet and lowest triplet states depends differently on the irradiance in comparison with the photobleaching in higher states. The first channel is characterized by a quadratic intensity dependence in contrast to the second channel that shows a cubic dependence. The competition between these photobleaching channels is very sensitive to the rate constants as well as to the repetition rate, the pulse duration, and the peak intensity. The double-exponential decay of the fluorescence is explained by the spatial inhomogeneity of the light beam. The findings in this work are discussed in terms of the possibility of using many-photon-induced photobleaching for new three-dimensional read−write devices.

I. Introduction

Nonlinear optics is an important area of contemporary science and technology. Nowadays, pulsed lasers with high peak intensities are widely used in different optical devices, where the high brilliance of the laser and the accompanying many-photon absorption drastically affect the photochemical properties of the studied samples. In general, absorption and emission coefficients as well as the photostability of a material dictate the suitability for any kind of application. One of the processes that reduces the photostability is photobleaching caused by photochemical reactions that remove molecules from the absorption−emission cycle. Often the photobleaching constitutes an unwanted effect in various fluorescent-based detection experiments. For example, the use of multiphoton-induced confocal fluorescence microscopy is often limited by increased photobleaching[1,2] due to the decrease of the amount of fluorescence photons and, hence, the decrease of the sensitivity and accuracy of measurements. However, the photobleaching is not only undesirable: The photostability of a fluorescent dye related to the photobleaching also can be utilized in various applications, such as single-molecule detection.[3−5] Accordingly, photobleaching recently has been employed by several groups[6−9] as a recording mechanism in three-dimensional (3D) optical memory materials. In fact, the design of 3D data storage memories has also been based on multiphoton absorption, which could be of either a two-[6,8,9] or a three-photon nature.[7] Depending on the number of photons involved, the quality of the spatial resolution changes, which overall affects the efficiency of device fabrication. For example, because two-photon absorption depends quadratically on the excitation intensity, the confinement will be limited to a small volume, while in the case of three-photon absorption the confinement will be even better as it depends cubically on the excitation intensity and so on. This particular aspect of multiphoton absorption has been used as a means for activating chemical/physical processes with high resolution in three dimensions.[10] However, the improvement due to the nonlinear excitation is limited because of an increased focal spot caused by an increase of the wavelength. Detailed experimental and theoretical studies of photobleaching and laser-induced fluorescence can be found in recent articles by Eggeling et al.[11,12] The authors of this article minimize the photobleaching using multicolor pulsed excitation.

An important parameter that strongly influences the interaction between light and matter is the duration of the interaction. This duration is large when a periodical sequence of the laser pulses is used. In this case light populates to a significant degree the lowest triplet state that has a long lifetime. One can here mention the recent study of photobleaching using periodical short laser pulses by Polyzos et al.[13] applied on different pyrylium salts. One observed in that work a double-exponential dynamics of photobleaching through fluorescence detection and furthermore that the photobleaching rates for different pyrylium salts had different intensity dependences. As experimental data unambiguously indicate, the photoexcitation in one of the lower singlet states occurs due to two-photon absorption. After that the laser beam can excite the molecule to a higher singlet state or to a higher excited triplet state due to the rather strong population of the lowest triplet state. The photobleaching can thus happen in the excited singlet states as well as in the triplet

* Author to whom correspondence should be addressed. E-mail: gavri@theochem.kth.se.

† Permanent address: Department of Physics, Rostov State University of Transport Communication, Rostov-on-Don 344038, Russia.

10.1021/jp074756x CCC: $37.00
Published on Web 11/03/2007

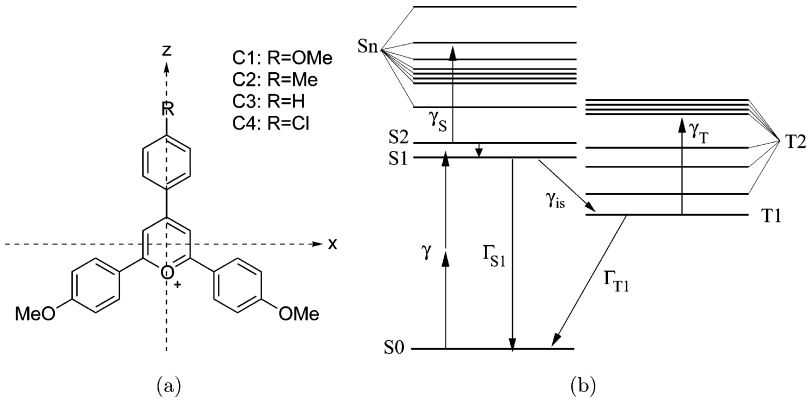

Figure 1. (a) Chemical structure of the pyrylium-based molecules discussed in this work. Me is the methyl CH_3 group. The C1 molecule is 4-methoxyphenyl-2,6-bis(4-methoxyphenyl) pyrylium tetrafluorobate. (b) Energy level scheme of the C1 molecule.

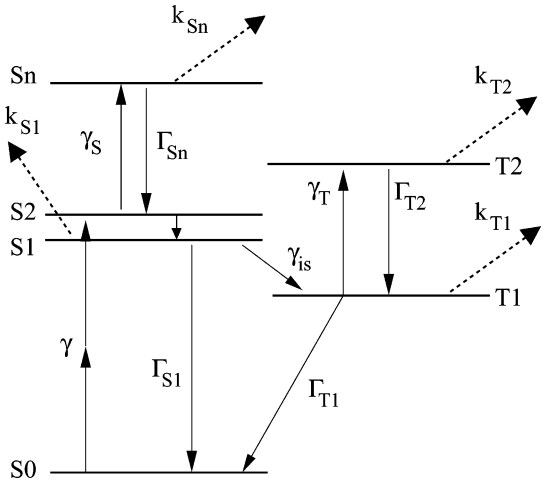

Figure 2. Simplified scheme of transitions.

states. To understand the dynamics of this photochemical process induced by multiphoton absorption, we have performed numerical simulations of photobleaching in pyrylium salts. Our model, based on stepwise absorption, includes the photobleaching in the first singlet and triplet states as well as in the manifolds of higher excited singlet and triplet states. In the numerical simulations, we select the representative pyrylium salt, 4-methoxyphenyl-2,6-bis(4-methoxyphenyl) pyrylium tetrafluorobate, as studied in the experimental work.[13] The main aim of our study is thus to explain the results of the measurements of Polyzos et al.[13] and to develop a detailed theory of photobleaching taking into account the temporal shape of the laser beam. To explain the observed[13] double-exponential decay of fluorescence, we consider the spatial inhomogeneity of the light beam. We believe that the mechanism of photobleaching can be different in the high- and low-intensity regions of the beam.

The paper is organized as follows. We start in section II from the physical model of the interaction of a periodical sequence of short pulses with few-level molecules with singlet and triplet subsystems. The analysis and solution of the rate equations are presented in section IIA. The computational details can be found in section III. The results of the numerical simulations of the photodynamics of the pyrylium salt and of the laser-induced fluorescence are analyzed in section IV. Our findings are summarized in section V.

II. Formulation of the Theory

To explain the results of the experiment,[13] we consider the propagation of a periodic sequence of short light pulses in nonlinear media containing pyrylium salt molecules (Figure 1a). Let us start from a simplified scheme of transitions depicted in Figure 2. This scheme selects the principal channels playing key roles in the photobleaching process. The kinetics of spectral transitions accompanied by photobleaching obey the following rate equations for the populations of singlet and triplet states involved in the studied process

$$\frac{\partial}{\partial t}\rho_{S_0} = -\gamma(t)(\rho_{S_0} - \rho_{S_1}) + \Gamma_{S_1}\rho_{S_1} + \Gamma_{T_1}\rho_{T_1}$$

$$\frac{\partial}{\partial t}\rho_{S_1} = \gamma(t)(\rho_{S_0} - \rho_{S_1}) - \gamma_S(t)(\rho_{S_1} - \rho_{S_n}) - (\Gamma_{S_1} + \gamma_{is} + k_{S_1})\rho_{S_1} + \Gamma_{S_n}\rho_{S_n}$$

$$\frac{\partial}{\partial t}\rho_{S_n} = \gamma_S(t)(\rho_{S_1} - \rho_{S_n}) - (\Gamma_{S_n} + k_{S_n})\rho_{S_n}$$

$$\frac{\partial}{\partial t}\rho_{T_1} = \gamma_{is}\rho_{S_1} - (\Gamma_{T_1} + k_{T_1})\rho_{T_1} + \Gamma_{T_2}\rho_{T_2} - \gamma_T(t)(\rho_{T_1} - \rho_{T_2})$$

$$\frac{\partial}{\partial t}\rho_{T_2} = -(\Gamma_{T_2} + k_{T_2})\rho_{T_2} + \gamma_T(t)(\rho_{T_1} - \rho_{T_2})$$

$$\frac{\partial}{\partial t}\rho_b = k_{S_1}\rho_{S_1} + k_{S_n}\rho_{S_n} + k_{T_1}\rho_{T_1} + k_{T_2}\rho_{T_2} \qquad (1)$$

Here ρ_{S_0}, ρ_{S_1}, ρ_{T_1}, and ρ_{T_2} are the S_0, S_1, T_1, and T_2 level populations, respectively, ρ_b is the concentration of bleached molecules, $\gamma(t)$ is the rate of two-photon (TP)-induced transition $S_0 \rightarrow S_1$, $\gamma_S(t)$ and $\gamma_T(t)$ are the rates of one-photon-induced transitions $S_1 \rightarrow S_n$ and $T_1 \rightarrow T_2$, γ_{is} is the rate of intersystem crossing (ISC) interaction, Γ_{S_1}, Γ_{S_n}, Γ_{T_1}, and Γ_{T_2} are the decay rates of the S_1, S_n, T_1, and T_2 states, respectively, and k_{S_1}, k_{S_n}, k_{T_1}, and k_{T_2} are the bleaching rates from the corresponding states. It is worthwhile to note that in the general case the intersystem crossings S_n-T_2 and T_2-S_n have to be taken into account.[11] We assume that the initial concentration of the molecules $\rho_{S_0}(t = 0) = 1$ is normalized to one, except in the field eq 34. The rate of the TP population of the S_1 (or S_2) level is defined by the cross-section of two-photon absorption (TPA) and depends quadratically on the radiation intensity $I(t)$

$$\gamma(t) = \frac{\sigma_2 I^2(t)}{2\hbar\omega}\frac{\Gamma^2}{(2\omega - \omega_{S_1S_0})^2 + \Gamma^2} \qquad (2)$$

where the photon frequency is tuned in resonance with the TPA transition $\omega \approx \omega_{S_1,S_0}/2$ and where Γ is a homogeneous

broadening of the spectral line. The rate of the T_1-T_2 one-photon transition depends linearly on $I(t)$

$$\gamma_T(t) = \frac{(\mathbf{e}\cdot\mathbf{d}_{T_2T_1})^2 I(t)}{\hbar^2 c\epsilon_0}\frac{\Gamma}{(\omega-\omega_{T_2T_1})^2+\Gamma^2} \approx \frac{\sigma_1 I(t)}{\hbar\omega}\frac{\Gamma^2}{(\omega-\omega_{T_2T_1})^2+\Gamma^2} \quad (3)$$

where $\mathbf{d}_{T_2T_1}$ is a dipole moment of the transition T_1-T_2. The rate of the $S_1 \rightarrow S_n$ one-photon transition $\gamma_S(t)$ is given the same expression (eq 3) after the replacement of $\mathbf{d}_{T_2T_1} \rightarrow \mathbf{d}_{S_nS_1}$ and $\omega_{T_2T_1} \rightarrow \omega_{S_1S_n}$. As we study randomly oriented molecules, we have to perform orientational averaging of the transition dipole moment relative to the polarization vector of the light $\mathbf{e}$. We replace approximately $(\mathbf{e}\cdot\mathbf{d}_{T_2T_1})^2$ by $d_{T_2T_1}^2/3$ and use conventional orientationally averaged cross-sections[14] of two-photon (σ_2) and one-photon $\sigma_1 = d_{T_2T_1}^2\omega/(3\hbar c\epsilon_0\Gamma)$ absorption.

Our simulations show that the TPA cross-section is larger for the $S_0 \rightarrow S_2$ TPA transition (see Table 2, Figure 2, and discussion below). However, even for resonant excitation of the level S_2, this level is quenched with a rate $\sim 10^{12}$ s^{-1} higher than the rate of quenching of the S_1 level Γ_{S_1} of $\sim 10^8-10^9$ s^{-1}. Due to this circumstance, mainly the S_1 level is populated, and one can restrict the analysis, taking into account only this level.

The two-photon transition $S_0 \rightarrow S_1$ is rather weak. This allows us to neglect the saturation of this transition; the saturation of the $S_1 \rightarrow S_n$ and $T_1 \rightarrow T_2$ one-photon transitions is also neglected because it is small for intensities used in our simulations

$$\rho_{S_0} - \rho_{S_1} \approx \rho_{S_0} \quad \rho_{S_1} - \rho_{S_n} \approx \rho_{S_1} \quad \rho_{T_1} - \rho_{T_2} \approx \rho_{T_1} \quad (4)$$

This happens when

$$\gamma \ll \Gamma_{S_1} \quad \gamma_S \ll \Gamma_{S_n} \quad \gamma_T \ll \Gamma_{T_2}$$

or

$$(2\gamma + \Gamma_{S_1})\tau \ll 1 \quad (2\gamma_S + \Gamma_{S_n})\tau \ll 1 \quad (2\gamma_T + \Gamma_{T_2})\tau \ll 1 \quad (5)$$

However, the "saturation" of the $S_0 \rightarrow S_1 \rightarrow T_1$ sequential transition should be taken into account explicitly due to the possible significant population of the lowest triplet state. This happens because of the small decay rate of the T_1 state and, hence, the rather significant storage of the molecules in the lowest triplet state $\rho_{T_1} \propto N$, which is proportional to the number of pulses N during the lifetime of the lowest triplet state (eq 15).

The separation between pulses $\Delta \approx 12$ ns is longer than the lifetimes of the excited singlet and triplet states. This means that the levels S_1, S_n, and T_2 are depopulated almost completely at the instant $t = n\Delta$ ($n = 0, 1, ...$) before the next pulse (Appendix A), because

$$\exp(-(\Gamma_{S_1} + k_{S_1} + \gamma_{is})\Delta) \ll 1 \quad \exp(-(\Gamma_{S_n} + k_{S_n})\Delta) \ll 1 \quad \exp(-(\Gamma_{T_2} + k_{T_2})\Delta) \ll 1 \quad (6)$$

Due to this circumstance, the particle conservation law $\rho_{S_0}(t) + \rho_{S_1}(t) + \rho_{S_n}(t) + \rho_{T_1}(t) + \rho_{T_2}(t) + \rho_b(t) = 1$ reads at the instant $t = n\Delta$ (see also Appendix A)

$$\rho_{S_0}{}^n + \rho_{T_1}{}^n + \rho_b{}^n \approx 1 \quad (7)$$

We use here and below a special notation for the density matrix, $\rho^n = \rho(t = n\Delta - 0)$, at the instant $t = n\Delta$ just before the nth pulse.

A. Solution of the Rate Equations for a Sequence of Periodical Pulses. We solve eq 1 for the periodical sequences of short pulses. We model the single pulse by a rectangular shape and use the fact that the duration of the single pulse $\tau =$ 100 fs is essentially shorter than all characteristic times. The rectangular shape of a single pulse allows us to solve the kinetic eq 1 analytically. To solve these equations, we use the fact that the studied system is characterized by the fast relaxation of excited singlet and T_2 states and slower relaxation of the T_1 state, $\tau_{ST} \approx \Gamma_{T_1}{}^{-1} \gg \Gamma_{S_1}{}^{-1}, \Gamma_{S_n}{}^{-1}, \Gamma_{T_2}{}^{-1}$. The dynamics of photobleaching characterized by the time τ_B are much slower, $\tau_B \gg \tau_{ST}$. A strict definition of τ_{ST} and τ_B will be given below. We divide the solution of these equations into three steps. First of all, we describe the rather slow dynamics of population of the lowest triplet state, solving the coupled eq 1 for ρ_{S_0}, ρ_{S_1}, ρ_{T_1}, and ρ_{T_2} as outlined in Appendix A. The second step is the solution of the coupled equations for the populations of S_1 and S_n states (eq 1), which are proportional to the slowly varying population of the ground state $\rho_{S_0}(t)$. We leave out the discussion of this simple but rather lengthy derivation and with a final result that is quite similar to the expressions for the triplet states (eq A3). The solution of the population equation for the photobleached molecules $\rho_b(t)$ constitutes the final step.

The population of the first excited state at the end of the nth pulse, $\rho_{S_1}(n\Delta + \tau)$ is given by eq 1. The solution of this equation is straightforward

$$\rho_{S_1}(n\Delta + \tau) = \gamma\phi(\tau)\rho_{S_0}(n\Delta) \approx \gamma\tau\rho_{S_0}(n\Delta) \quad (8)$$

where $\phi(\tau) \approx (1 - \exp[-\tau(2\gamma + \bar{\Gamma}_{S_1})])/(2\gamma + \bar{\Gamma}_{S_1}) \approx \tau$ for the studied case of a sequence of short pulses $\bar{\Gamma}_{S_1} \equiv \Gamma_{S_1} + k_{S_1} + \gamma_{is} \ll 1/\tau$. Here $\gamma\tau$ is the fraction of the molecules excited in the S_1 state during one pulse. We use here and below special notations for the peak values of the intensity $I(t) \rightarrow I$ and for the peak values of the rates of radiative transitions $\gamma(t) \rightarrow \gamma$, $\gamma_S(t) \rightarrow \gamma_S$, and $\gamma_T(t) \rightarrow \gamma_T$.

Now we are at the stage to find the populations of the ground and the first triplet states. The populations between the nth and the $(n + 1)$th pulses obey eq 1 with $\gamma(t) = 0$. The solution of these equations results in the following recurrent equation (and its solution) for the population $\rho_{S_0}{}^n$ at the instant $t = n\Delta - 0$ before the nth pulse (Appendix A)

$$\rho_{S_0}{}^n = (1 - \rho_b{}^n)R^n \quad R^{n+1} = 1 - e^{-\tilde{\Gamma}_{T_1}\Delta} + \lambda R^n \quad (9)$$

where we introduced the branching ratio of the intersystem crossing

$$\phi_{isc} = \frac{\gamma_{is}}{\Gamma_{S_1} + \gamma_{is} + k_{S_1}} \quad \lambda = (1 - \phi_{isc}\gamma\tau)\, e^{-\tilde{\Gamma}_{T_1}\Delta} < 1 \quad (10)$$

One can see that the dynamics depend on the total rate of depopulation of the T_1 state through three channels: the radiative and nonradiative decay $T_1 \rightarrow S_0$, the photobleaching in the T_1 level, and the excitation to the T_2 state with the following photobleaching

$$\tilde{\Gamma}_{T_1} = \Gamma_{T_1} + k_{T_1} + \frac{\alpha}{\Delta} \quad \alpha = \gamma_T\tau æ_{T_2} \quad æ_{T_2} = \frac{k_{T_2}}{\Gamma_{T_2} + k_{T_2}} \quad (11)$$

The solution ($R^n = \lambda^n p + q$) of the recurrent eqs 9 and 7 results in the following expressions for the populations of the lowest singlet and triplet states

$$\rho_{S_0}{}^n = [1 - p(1 - e^{-n\Delta/\tau_{ST}})](1 - \rho_b{}^n)$$
$$\rho_{T_1}{}^n = p(1 - e^{-n\Delta/\tau_{ST}})(1 - \rho_b{}^n) \quad (12)$$

The parameters

$$q = \frac{e^{\tilde{\Gamma}_{T1}\Delta} - 1}{\phi_{isc}\gamma\tau + e^{\tilde{\Gamma}_{T1}\Delta} - 1} \approx \frac{(\Gamma_{T_1} + k_{T_1})\Delta + \gamma_T æ_{T_2}\tau}{(\Gamma_{T_1} + k_{T_1})\Delta + (\gamma\phi_{isc} + \gamma_T æ_{T_2})\tau}$$

$$p = 1 - q = \frac{\phi_{isc}\gamma\tau}{\phi_{isc}\gamma\tau + e^{\tilde{\Gamma}_{T1}\Delta} - 1} \approx \frac{\gamma\tau\phi_{isc}}{(\Gamma_{T_1} + k_{T_1})\Delta + (\gamma\phi_{isc} + \gamma_T æ_{T_2})\tau} \quad (13)$$

found from initial conditions, $\rho_{S_0}{}^0 = 1$ and $\rho_b{}^0 = 0$, have simple physical meanings when the photobleaching is neglected: q is the ground-state population while p is the population of the T_1 state for $t \to \infty$.

As one can discern from eq 12, the quasi-stationary distribution of populations $\rho_{S_0}(t) \approx q(1 - \rho_b(t))$ and $\rho_{T_1}(t) \approx p(1 - \rho_b(t))$ is settled during $\tau_{ST} = -\Delta/\ln \lambda < 1/\Gamma_{T_1}$

$$\tau_{ST} \approx \frac{1}{\Gamma_{T_1} + k_{T_1} + (\gamma\phi_{isc} + \gamma_T æ_{T_2})\tau/\Delta} \quad (14)$$

Later on the photobleaching starts to decrease the number of resonant molecules and $\rho_{S_0}(t) \to 0$ because all molecules are photobleached $\rho_b(t) \to 1$ when $t \to \infty$ (see below). It is relevant to mention that $\tau_{ST} \approx 1/\tilde{\Gamma}_{T_1}$ (eq 14) is defined only by the lifetime of the T_1 state when $\phi_{isc}\gamma\tau \ll \tilde{\Gamma}_{T_1}\Delta$, while $\tau_{ST} \approx \Delta/\gamma\tau\phi_{isc}$ depends on the pump intensity in the opposite case $\phi_{isc}\gamma\tau \gg \tilde{\Gamma}_{T_1}\Delta$.

The physical meaning of eq 12 deserves special comment. Usually $\tilde{\Gamma}_{T_1}\Delta \ll 1$. In this case, the population of the lowest triplet state

$$p = N(T_1)N \quad N = \tau_{T_1}/\Delta \quad (15)$$

is equal to the population of the T_1 state created by a single pulse $N(T_1) = \phi_{isc}\gamma\tau q$ times the number of pulses N during the lifetime of the triplet state $\tau_{T_1} = 1/\tilde{\Gamma}_{T_1}$. N is the factor of accumulation of the particle in the T_1 state. Here $\gamma\tau q$ is the population of the first excited singlet state just after a single pulse (eqs 8 and 13). Equation 15 indicates that the ground state is completely depopulated due to optical pumping of the triplet state $p \approx 1$ when the number of transitions $S_0 \to T_1$ due to TPA and intersystem crossing per pulse $\phi_{isc}\gamma\tau$ significantly exceeds the number of decay events of the triplet state $\tilde{\Gamma}_{T_1}\Delta$.

B. Rate of Photobleaching. From the derivation above, we are now in the position to find the concentration of bleached molecules. From eq 1 for $\rho_b(t)$ we have

$$\rho_b{}^{n+1} - \rho_b{}^n = \int_{n\Delta}^{(n+1)\Delta}(k_{T_1}\rho_{T_1}(t) + k_{T_2}\rho_{T_2}(t) + k_{S_1}\rho_{S_1}(t) + k_{S_n}\rho_{S_n}(t))\,dt \quad (16)$$

The second integral at the right-hand side of this equation was solved already (eqs A2 and A4). The population $\rho_{T_1}(t) \approx$ constant during Δ because τ_{ST} and the time of photobleaching is significantly longer than Δ. Due to this circumstance, $\int_{n\Delta}^{(n+1)\Delta} \rho_{T_1}(t)\,dt \approx \rho_{T_1}{}^n\Delta$. We omit the rather lengthy but simple solution of eq 1 for $\rho_{S_1}(t)$ and $\rho_{S_n}(t)$, which is similar to the solution of the rate equation for $\rho_{T_2}(t)$ (eq A3). The substitution of $\rho_{S_1}(t)$ and $\rho_{S_n}(t)$ in eq 16 results in

$$\rho_b{}^{n+1} - \rho_b{}^n = (k_{T_1}\Delta + æ_{T_2}\gamma_T\tau)\rho_{T_1}{}^n + \left(\frac{k_{S_1}\gamma\tau}{\Gamma_{S_1} + k_{S_1} + \gamma_{is}} + \frac{k_{S_n}\gamma\gamma_S\varphi(\tau)}{\Gamma_{S_n} + k_{S_n}}\right)\rho_{S_0}{}^n \quad (17)$$

where the photobleaching in the S_n state depends quadratically on the pulse duration in the studied case of short pulses (see also eq 8)

$$\varphi(\tau) = \frac{1}{\Gamma_{S_n} + k_{S_n} + 2\gamma_S}\left[\tau - \frac{1 - e^{-\tau(\Gamma_{Sn} + k_{Sn} + 2\gamma_S)}}{\Gamma_{S_n} + k_{S_n} + 2\gamma_S}\right] \approx \frac{\tau^2}{2} \quad (18)$$

Taking into account the expression for $\rho_{S_0}{}^n$ and $\rho_{T_1}{}^n$ (eq 12) and making a transition to the continuum variable $t = n\Delta$, we obtain

$$\frac{\partial\rho_b(t)}{\partial t} = \left\{\left(k_{T_1} + æ_{T_2}\gamma_T\frac{\tau}{\Delta}\right)p(1 - e^{-t/\tau_{ST}}) + \frac{1}{\Delta}\left(\frac{k_{S_1}\gamma\tau}{\Gamma_{S_1} + k_{S_1} + \gamma_{is}} + \frac{k_{S_n}\gamma\gamma_S\tau^2}{2(\Gamma_{S_n} + k_{S_n})}\right)[1 - p(1 - e^{-t/\tau_{ST}})]\right\}(1 - \rho_b(t)) \quad (19)$$

The integration of this equation gives straightforwardly

$$\rho_b(t) = 1 - \exp\left[-\frac{1}{\tau_B}(t - \chi(t))\right] \quad (20)$$

where the rate of photobleaching

$$\frac{1}{\tau_B} = p\left(k_{T_1} + æ_{T_2}\gamma_T\frac{\tau}{\Delta}\right) + q\frac{\gamma\tau}{\Delta}(æ_{S_1} + \gamma_S\tau æ_{S_n}/2) \quad (21)$$

is a sum of effective rates of photobleaching in the T_1, T_2, S_1, and S_n states. It is necessary to note that the photobleaching is characterized by a single time of photobleaching, which includes the photobleaching in all states. Here

$$æ_{S_1} = \frac{k_{S_1}}{\Gamma_{S_1} + k_{S_1} + \gamma_{is}}$$

and

$$æ_{S_n} = \frac{k_{S_n}}{\Gamma_{S_n} + k_{S_n}} \quad (22)$$

are the branching ratios (relative rates of bleaching processes from the S_1 and the S_n levels, respectively). A similar branching ratio $æ_{T_2}$ for the T_2 state is defined by eq 11.

In agreement with recent measurements,[12] the photobleaching in the triplet states is suppressed when the repetition rate $f_r = 1/\Delta$ is sufficiently low. Indeed, in this case the population of the T_1 level is exponentially small

$$p \approx \phi_{isc}\gamma\tau e^{-\tilde{\Gamma}_{T1}\Delta} \quad \tilde{\Gamma}_{T_1}\Delta \ll 1$$

TABLE 1: Excited-State Transition Dipole Moments (in a.u.) and Excitation Energies, $\hbar\omega_e$ (in eV), for 4-Methoxyphenyl-2,6-bis(4-methoxyphenyl) Pyrylium Tetrafluorobate Molecule Calculated at the TD-B3LYP/6-31G Level[a]**

	S−S					T−T			
	X	*Y*	*Z*	$\hbar\omega_e$		*X*	*Y*	*Z*	$\hbar\omega_e$
$d_{S_0S_1}$	0.5750	2.5989	−0.0029	2.65	$d_{T_1T_2}$	−1.6389	−0.0302	0.5151	0.28
$d_{S_0S_2}$	3.1113	−0.5340	−0.0094	2.86	$d_{T_1T_3}$	−1.0606	−0.0254	−0.0851	0.67
$d_{S_1S_3}$	−2.5748	−0.0071	0.0105	0.71	$d_{T_1T_4}$	−3.1266	−0.0697	−0.1311	0.91
$d_{S_1S_4}$	−0.1750	−0.0057	0.1859	1.02	$d_{T_1T_5}$	0.0389	0.0036	−0.0383	1.39
$d_{S_1S_5}$	−0.2683	0.0199	−0.0151	1.06	$d_{T_1T_6}$	0.0226	−0.0153	−0.8802	1.43
$d_{S_1S_6}$	0.1619	0.0147	−0.0408	1.08	$d_{T_1T_7}$	−0.1758	−0.0212	−0.4170	1.50
$d_{S_1S_7}$	−0.0689	0.0009	0.2117	1.12	$d_{T_1T_8}$	−0.0386	0.0088	0.2140	1.53
$d_{S_1S_8}$	0.1327	0.0211	0.0135	1.35					
$d_{S_1S_9}$	0.0417	−0.0053	−0.2973	1.60					
$d_{S_1S_{10}}$	0.0843	0.0251	0.6737	2.09					
$d_{S_2S_3}$	−0.0128	0.0428	2.8679	0.50					
$d_{S_2S_4}$	−0.3764	0.0506	0.0443	0.81					
$d_{S_2S_5}$	−0.0110	0.0320	0.3700	0.85					
$d_{S_2S_6}$	0.3751	−0.0182	0.0097	0.87					
$d_{S_2S_7}$	1.3115	0.0336	0.0212	0.91					
$d_{S_2S_8}$	0.0402	0.0164	0.7212	1.14					
$d_{S_2S_9}$	0.7414	0.0013	−0.0093	1.39					
$d_{S_2S_{10}}$	−0.2487	0.0085	0.0063	1.88					

[a] $E_{T_1} - E_{S_0} = 1.88$ eV

The duration of population of the T_1 state (τ_{ST}) affects only slightly the dynamics of the photobleaching through the term

$$\chi(t) = \tau_{ST}(1 - e^{-t/\tau_{ST}})\frac{1-\mu}{1+\mu q/p} \quad \mu = \frac{\gamma\tau æ_{S_1} + \gamma\gamma_S\tau^2 æ_{S_n}/2}{k_{T_1}\Delta + æ_{T_2}\gamma_T\tau} \tag{23}$$

Indeed, $\chi(t) \propto \tau_{ST}$ is important only at the initial step $t \lesssim \tau_{ST}$, where $\rho_b(t) \ll 1$. This means that the long-range dynamics of the photobleached and intact molecules by a periodical sequence of the pulses is defined by the equation

$$\rho_b(t) \approx 1 - e^{-t/\tau_B} \quad \rho(t) \approx e^{-t/\tau_B} \quad \tau_{ST} \ll \tau_B \tag{24}$$

Equation 21 shows that the photobleaching in the S_1 and T_1 states gives a linear dependence of the photobleaching rate on the pulse duration (since $p \propto \tau$ (eq 13)), contrary to the excited S_n and T_2 states, which lead to a quadratic dependence on τ.

Let us write down the full expression for τ_B

$$\frac{1}{\tau_B} = \frac{\gamma\tau[\phi_{isc}(k_{T_1} + æ_{T_2}\gamma_T\tau/\Delta) + (\Gamma_{T_1} + k_{T_1} + æ_{T_2}\gamma_T\tau/\Delta)(æ_{S_1} + \gamma_S\tau æ_{S_n}/2)]}{\Delta[\Gamma_{T_1} + k_{T_1} + (\gamma\phi_{isc} + \gamma_T æ_{T_2})\tau/\Delta]} \tag{25}$$

1. Long Pulse. It is interesting to compare our solution for a periodical sequence of pulses with the dynamics of photobleaching for a long single pulse

$$\rho_b(t) \approx 1 - \exp\left(-\int_0^t \frac{dt_1}{\tau_B(t_1)}\right)$$

$$\frac{1}{\tau_B(t)} = \frac{\gamma(t)\phi_{isc}[\gamma_T(t)æ_{T_2} + k_{T_1}]}{\Gamma_{T_1} + k_{T_1} + \gamma(t)\phi_{isc} + \gamma_T(t)æ_{T_2}} \tag{26}$$

To avoid unnecessary complexity, we write down this expression neglecting the photobleaching from the S_1 and S_n levels. One can see that the time of photobleaching (eq 25) coincides with the time of photobleaching (eq 26) for a long single pulse when $\tau = \Delta$. Indeed, in this case the sequence of pulses becomes a single pulse. The population of the lowest triplet state by a long pulse

$$\rho_{T_1}(t) \approx \frac{(1 - \rho_b(t))\gamma(t)\phi_{isc}}{\Gamma_{T_1} + k_{T_1} + \gamma(t)\phi_{isc} + \gamma_T(t)æ_{T_2}} \tag{27}$$

can also be significant due to the small relaxation rate of this state Γ_{T_1}. The ground state is depopulated according to eq 7.

C. Many-Level Molecule. The theory developed in the previous section is based on a simplified few-level scheme (Figure 2). However, simulations (Table 1 and Figure 1b) indicate that the studied molecule is essentially a many-level system. First of all, we have two close-lying excited states S_1 and S_2, which we discussed already in section II and which can be replaced by one state.

Figure 1b and Table 1 indicate that many of the excited triplet states can be reached from the T_1 level. We would like to remind the reader that only one excited triplet state T_2 is taken into account in section IIA. Let us therefore here take into account the excited-state absorption by a manifold of excited triplet states T_2 (Figure 1b). This is important for the one-photon $T_1 \rightarrow T_2$ transitions. Let us generalize eqs 1 for ρ_{T_1} and ρ_{T_2} for many excited triplet states (saturation is then neglected)

$$\frac{\partial}{\partial t}\rho_{T_1} = \gamma_{is}\rho_{S_1} - (\Gamma_{T_1} + k_{T_1})\rho_{T_1} + \sum_{T_2}\Gamma_{T_2}\rho_{T_2} - \sum_{T_2}\gamma_T(t)\rho_{T_1}$$

$$\frac{\partial}{\partial t}\sum_{T_2}\rho_{T_2} = \sum_{T_2}\gamma_T(t)\rho_{T_1} - \sum_{T_2}(\Gamma_{T_2} + k_{T_2})\rho_{T_2} \tag{28}$$

Assuming that the relaxation constants Γ_{T_2} and k_{T_2} ($k_{T_2} \ll \Gamma_{T_2}$) are the same for all T_2 levels, we again obtain eq 1 where ρ_{T_2} and γ_T now are the total populations of the excited triplet states. The total rates of one-photon transitions are then

$$\rho_{T_2} \rightarrow \sum_{T_2}\rho_{T_2} \quad \gamma_T(t) \rightarrow \sum_{T_2}\gamma_T(t) \tag{29}$$

This means that the results obtained in the previous sections for a single T_2 level are valid for the many-level case as well after the replacement $\gamma_T(t)$ (eq 3) by the total rate of the $T_1 \rightarrow T_2$ transition (eq 29).

TABLE 2: Input Data for Simulations[a]

σ_2 (S_1) (m^4/W)	σ_2 (S_2) (m^4/W)	ϕ_f	γ_{is}	Γ_{S_1}	$\Gamma^r_{T_1}$	Γ_{T_1}	Γ_{T_2}, Γ_{S_n}	k_{T_1}, k_{S_1}	k_{T_2}, k_{S_n}	τ (fs)	f_r (MHz)
0.95×10^{-37}*	1.24×10^{-37}*	0.68	10^6	3.33×10^8	*0.047	10^5	10^{12}	107	10^6	100	82

[a] $\Gamma = 0.1$ eV, $\Delta = 1/f_r \approx 12$ ns. The rate constants are given in s^{-1}. The calculated parameters are marked by asterisks.

Exactly the same reasons allow us to take into account one-photon transitions from S_1 to higher excited singlet states S_n by means of a replacement of ρ_{S_n} and $\gamma_S(t)$ to the total population of S_n levels and the total rate of the $S_1 \rightarrow S_n$ transition

$$\rho_{S_n} \rightarrow \sum_{S_n} \rho_{S_n} \quad \gamma_S(t) \rightarrow \sum_{S_n} \gamma_S(t) \tag{30}$$

It is necessary to note that this method of taking into account the manifold of excited singlet and triplet states ceases to be valid when the one-photon transitions approach saturation.

D. Cross-Sections of Nonlinear Absorption. The TP absorption $S_0 \rightarrow S_1$ is accompanied by the two-step three-photon absorption, $S_0 \rightarrow S_1$, with following $T_1 \rightarrow T_2$ and $S_1 \rightarrow S_n$. To obtain the cross-section of this photoabsorption σ_3^{eff} we use the relation between the rate of three-photon transition $W_3 = \sigma_3^{eff} I^3/(3\hbar\omega)$ and σ_3^{eff}. The rates $W_T(t)$ and $W_S(t)$ of radiative transitions from the ground to the excited states T_2 and S_n can be found directly from the kinetic eq 1

$$\frac{\partial}{\partial t}\rho_{T_2} = -(\Gamma_{T_2} + k_{T_2})\rho_{T_2} + W_T(t)\rho_{S_0}$$

$$\frac{\partial}{\partial t}\rho_{S_n} = -(\Gamma_{S_n} + k_{S_n})\rho_{S_n} + W_S(t)\rho_{S_0} \tag{31}$$

The expression for $W_T(t)$ is immediately obtained from eq 1 using the fact that $\rho_{T_1}/\rho_{S_0} \approx p/q$ as is seen from eqs 13 and 12. Similar calculations give the expression for $W_S(t)$. Finally, the total rate of three-photon transitions $S_0 \rightarrow T_2$ and $S_0 \rightarrow S_n$ reads

$$W_3 = W_T(t) + W_S(t) = \frac{\tau\phi_{isc}\gamma(t)\gamma_T(t)}{\tilde{\Gamma}_{T_1}\Delta} + \gamma(t)\gamma_S(t)\delta t$$

$$= \frac{\sigma_2}{2\hbar\omega}\left(\frac{\phi_{isc}p_{T_2T_1}}{\tilde{\Gamma}_{T_1}\Delta}\tau + p_{S_1S_n}\delta t\right)I^3(t) \tag{32}$$

Here $p_{T_2T_1} = \gamma_T(t)/I(t)$, $p_{S_1S_n} = \gamma_S(t)/I(t)$, and $\delta t = t - n\Delta$. We obtain the peak value of the cross-section at the end of a pulse

$$\sigma_3^{eff} = \frac{3\sigma_2\tau}{2}\left(\frac{\phi_{isc}p_{T_2T_1}}{\tilde{\Gamma}_{T_1}\Delta} + p_{S_1S_n}\right) \tag{33}$$

In the general case the intensity of the light decreases

$$\left(\frac{\partial}{\partial z} - \frac{1}{c}\frac{\partial}{\partial t}\right)I = -\mathcal{N}(\sigma_1 I + \sigma_2 I^2 + \sigma_3 I^3 + \cdots) = -\mathcal{N}(\sigma_1 I + \sigma(I)I^2) \tag{34}$$

due to one, two, three, ... photon absorption with the cross-sections σ_1, σ_2, σ_3, etc. Here $\mathcal{N}$ is the concentration of intact molecules per unit volume. In the studied system the TPA is accompanied by three-photon sequential absorption. To see how the three-photon absorption (eq 33) affects the two-photon absorption, it is convenient to introduce an effective cross-section of nonlinear absorption (2 + 3 photon absorption)

$$\sigma(I) = \sigma_2 + \sigma_3^{eff} I \tag{35}$$

TABLE 3: Excitation Energies, ω (in eV), and σ^{TPA} (in GM Units)[a]

		calculated		experimental[b]	
molecule	state	ω	σ^{TPA}	$\phi\sigma^{TPA}$	σ^{TPA}
C1	S_1	2.65	218		
	S_2	2.86	285	182	267
C2	S_1	2.62	177		
	S_2	2.99	471	513	675
C3	S_1	2.61	150		
	S_2	3.03	645	767	1278
C4	S_1	2.58	174		
	S_2	2.94	450	390	1772

[a] The TPA cross-sections are computed for $\Gamma = 0.1$ eV. [b] The experimental excitation energy is not given in the table as we do not know which excited state is involved.

The increase of nonlinear absorption due to strong population of the lowest triplet state is clearly important in optical limiting.

III. Computational Details

The rate equations are solved using as input parameters the TPA cross-sections, transition dipole moments of T_1-T_2 and S_1-S_n transitions, energies of the levels, as well as the rate constants. All parameters are collected in Tables 1 and 2. Except the rate constants, all spectroscopic parameters are computed using density functional response theory as outlined below.

The dynamics of the photobleaching and of the fluorescence of the many-level pyrylium salt molecule (Figure 1) are simulated using either the recurrent equations (eq A8) or the analytical solution (eq 20). The two approaches give almost the same results. The manifold of excited singlet and triplet states is taken into account as outlined in section IIC.

A. Spectroscopic Parameters Computed Using Density Functional Theory. We assume in the simulations that the photon frequency is tuned in resonance with the strongest TPA transition $S_0 \rightarrow S_2$: $2\omega = \omega_{S_2S_0}$.

1. Transition Energies, Dipole Moments, and Rates of Phosphorescence. Geometry optimization of the molecular system has been carried out using Becke's three-parameter hybrid functional (B3LYP)[15] at the polarized split-valence basis set 6-31G*.[16] The calculations of dipole moments and energies of the S_0-S_k ($k = 1$ or 2) transitions have been carried out using linear density functional response theory.[17] The remaining dipole moments for S_m-S_l, T_1-T_m ($m, l = 1, 2, 3, ...$) and spin-symmetry-forbidden T_p-S_0 ($p = 1$, 2, or 3) transitions have been performed using quadratic density functional response theory.[17,18] Apart from computing the transition dipole moments between various states of the investigated molecule we also carried out necessary computations of the TPA cross-sections, assuming that the photon frequency is tuned in resonance with the strongest TPA transition $S_0 \rightarrow S_2$; i.e., $2\omega = \omega_{S_2S_0}$. The results of these calculations are summarized in Tables 1 and 3. The presented results correspond solely to electronic transition moments, as we neglect vibrational degrees of freedom in our calculations completely. The Franck−Condon distribution reduces the intensity of the spectral transitions. We have mimicked this effect by reducing the transition dipole moments from Table 1 of the one-photon transitions by a factor of 2.

Our computations of the spin-symmetry-forbidden T_p-S_0 transitions predict the radiative rates (phosphorescence) of the $T_p \rightarrow S_0$ transitions for $p = 3$, 2, or 1: $1/\Gamma_{T_3-S_0}{}^r = 8.25912 \times 10^{-4}$ s, $1/\Gamma_{T_2-S_0}{}^r = 8.327$ s, and $1/\Gamma_{T_1}{}^r = 1/\Gamma_{T_1-S_0}{}^r = 21.37$ s. These results indicate that the first two triplet states, T_1 and T_2, are lying significantly below the first excited singlet state (Table 2), and, consequently, the radiative transition rates from these states are suppressed by having only a small spin−orbit coupling. Contrary to this, the third excited triplet state is positioned closely to S_1, and the radiative rate, $\Gamma_{T_3-S_0}{}^r$, is 3 orders of magnitude larger, as the spin−orbit coupling between the S_1 and T_3 states is efficient. Furthermore, due to the large spin−orbit coupling between these states, an effective intersystem crossing between the S_1 and the T_3 states is expected. Comparison with the total rate of the quenching of the first triplet state (Table 2) indicates that the radiative channel is negligibly small in comparison to the nonradiative one.

2. Role of Substituents on the Cross-Section of Two-Photon Absorption. In the experimental work by Polyzos et al.,[13] the investigation of photobleaching behavior was extended to a group of pyrylium salts. This group consists of molecules with the same basic chemical structure, differing only by specific substituents, as shown in the Figure 1a. The experiments[9] showed that changes in the nature of substituents leads to changes in the multiphoton absorption cross-sections. We calculated the TPA cross-sections[18,19] for these molecules. Details about the calculation method can be found in recent work.[20] As one can see from Table 3, the calculated cross-sections are in reasonable agreement with the experimental data for C1 and C2 molecules.

At this point, we draw the reader's attention to the calculated TPA cross-section reported in Table 3. From this table it is quite clear that the increase/decrease in TPA values is a strong function of the symmetry as well as of the substituents attached with it for a fixed backbone of the system. To make this point clear, if one looks at C1, then one immediately notices the symmetry present in this system due to the attachment of the same group (methoxy group). Due to the symmetry present in the C1 molecule, the charge transfer and the transition moment direction are parallel, which is not the case for other members of this family, such as C2, C3, and C4. Hence the TPA cross-section is the smallest for C1 among the members of this family. The change in the TPA cross-sections for the other molecules is due to the strength of electron-releasing/withdrawing groups. The change of susbtituents leads to a change in the transition dipole moment between the ground and the excited states, which in turn dictates the change in the TPA cross-sections.[20] At this point, one can say that the mechanism involved in the enhancement of TPA cross-sections and, hence, in photobleaching is expected to remain the same for this particular class of molecules. The possibility of involvement of other excited states can although not be ruled out, as the change in substituents could lead to drastic changes in the ordering of the energy levels. Hence, one needs to look at the singlet as well as the triplet manifolds of the system very carefully before making any conclusion regarding the mechanism that could affect photobleaching.

B. Empirical Rate Constants. Unfortunately, we are unable to compute the remaining part of the kinetic parameters, such as the rate constants and the photobleaching rates. Instead we choose these parameters analyzing available experimental data. The broadening of the spectral lines used in the simulations is $\Gamma = 0.1$ eV (see ref 21). We have chosen the total decay rates of the S_1 and T_2 states as $\Gamma_{S_1} = 3.33 \times 10^8$ s^{-1} and $\Gamma_{T_2} = 10^{12}$ s^{-1}, respectively. Experimental data for different pyrylium salts in different solvents show that $\Gamma_{S_1}{}^{-1} = 0.95-10$ ns,[22] $\Gamma_{S_1}{}^{-1} = 0.71-36$ ns,[23] and $\Gamma_{S_1}{}^{-1} = 2.7$ or 3.6 ns.[24] We did not find information about the relaxation rate of the T_2 state in the pyrylium salts. We have found only $\Gamma_{T_2}{}^{-1} = 0.2$ ps for rhodamine 6G.[2] We use in the simulations $\Gamma_{T_2}{}^{-1} = \Gamma_{S_n}{}^{-1} = 1$ ps.

Our simulations are very sensitive to the lifetime $\Gamma_{T_1}{}^{-1}$ of the T_1 state and the rate of the intersystem crossing γ_{is}. Experimental data for the pyrylium salts in different solvents show that $\Gamma_{T_1}{}^{-1} = 6.9$ or 9.6 μs (at room temperature)[24] and $\Gamma_{T_1}{}^{-1} = 5$ or 10 μs (at room temperature).[25] Tripathi et al.[22] claim that the lifetime of the first triplet state of some pyrylium salts is sensitive to the concentration of the solvent, $\Gamma_{T_1}{}^{-1} > 100$ μs at infinite dilution while $\Gamma_{T_1}{}^{-1} < 1$ μs for higher concentrations of the pyrylium molecules. It is worthwhile to mention that $\Gamma_{T_1}{}^{-1} = 2.6$ μs for rhodamine 6G.[2] The decrease of the temperature results in an prolongation of the lifetime of the T_1 state of the pyrylium salts up to $\Gamma_{T_1}{}^{-1} > 1$ ms ($T = 176$ K)[26] and $\Gamma_{T_1}{}^{-1} = 0.135-14$ s ($T = 77$ K).[23] The measurements discussed in the ref 13 were performed with pyrylium salts in the solid phase at room temperature. This motivates us to use in our simulations $\Gamma_{T_1}{}^{-1} \approx 10$ μs. We note that the lowest triplet states are mainly quenched nonradiatively $\Gamma_{T_1} = \Gamma_{T_1}{}^r + \Gamma_{T_1}{}^{nr} \approx \Gamma_{T_1}{}^{nr}$ at room temperature, while our simulations show that the radiative rate is very small (~ 1 s^{-1}, see section IIIA1).

Unfortunately, information on the rate of intersystem crossing is rather poor. Tripathi et al.[22] state that $\gamma_{is}/(\Gamma_{S_1} + \gamma_{is}) < 10\%$ for pyrylium salts. Eggeling et al. have found for rhodamine 6G that $\gamma_{is} = 7.3 \times 10^5$ s^{-1} (ref 3) and $\gamma_{is} = 1.1 \times 10^6$ s^{-1} (ref 2). We have chosen for our simulations $\gamma_{is} = 10^6$ s^{-1}. To conclude we should pay attention to the fluorescence yield $\phi_f = \Gamma_{S_1}^r/(\Gamma_{S_1}^r + \Gamma_{S_1}^{nr} + \gamma_{is} + k_{S_1})$. According to measurements of Polyzos et al. $\phi_f = 0.68$. Taking into account the above-mentioned data $\Gamma_{S_1} \approx 10^8-10^9$ s^{-1} and $\gamma_{is} \approx 10^6$ s^{-1} one can conclude that the nonradiative quenching (internal conversion) $\Gamma_{S_1}^{nr}$ of the first excited singlet state is comparable to the rate of radiative quenching $\Gamma_{S_1}^r$. This is a rather unexpected result, because the nonradiative channel is usually weaker than the radiative one for the first excited singlet state. For example, the analysis of Eggeling et al.[2] indicates that the relative rate of the nonradiative channel is about 5%.

The rates of photobleaching $k_{T_2} = 10^6$ s^{-1} and $k_{T_1} = 107$ s^{-1} are defined from the simulated rate of photobleaching $1/\tau_B$ (eq 25) using the measured value 2.9 s^{-1} (ref 13) for the intensity $I = 6 \times 10^{14}$ W/m^2 (see below). For k_{S_1} and k_{S_n}, we assumed, following Eggelling et al.,[2,3,11] that $k_{T_1} = k_{S_1} \ll k_{T_2}, k_{S_n}$. These studies demonstrate that higher levels are more photoreactive. It is necessary to note that the recent experimental data[12,27] indicate that the photobleaching in triplet states can be significantly faster than that in singlet states.

To make a comparison with the experiment of Polyzos et al.[7,9,13] we need to know the intensity used in these measurements, which, however, is not possible as this information is absent in these articles. We instead find the intensity using the formula

$$I = \frac{P\Delta}{\tau S} \tag{36}$$

where S is the area of illumination and P is the average irradiation power, which was varied[13] in the region $P \approx 1-10$ mW. We estimated the area of the illuminated spot from the article[9] as $S \approx 1$ μm $\times$ 1 μm. The experimental data collected

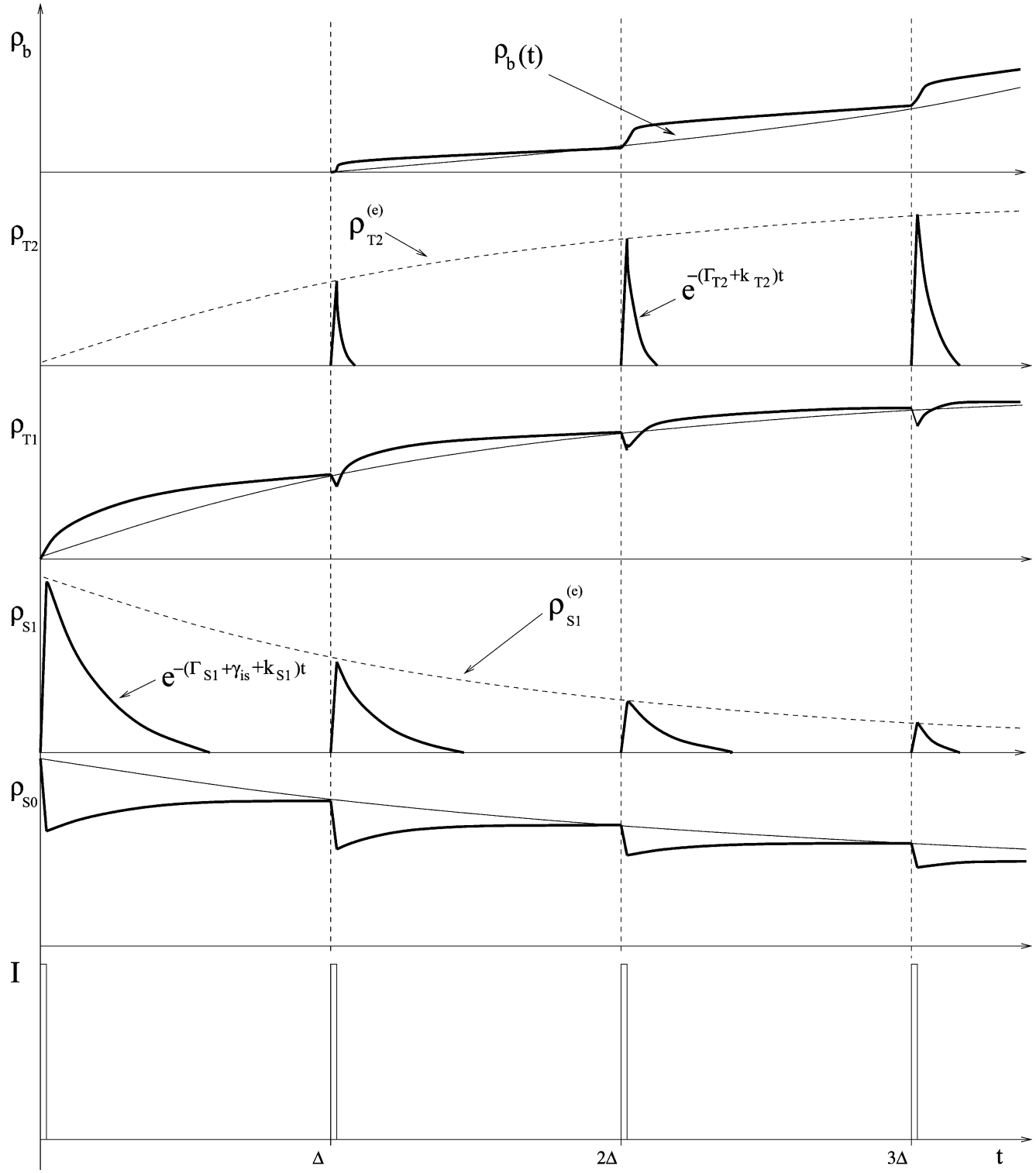

Figure 3. Schematic picture of the population dynamics. Envelopes of populations are drawn by dashed lines. The scale of population is different for different levels. (The amplitude of the peak in $\rho_{T_2}(\rho_{S_1})$ must be equal to the amplitude of the "hole" in $\rho_{T_1}(\rho_{S_0})$.)

in Table 1 of ref 13 are given for $P \approx 5$ mW, which corresponds according to eq 36 to $I \approx 6 \times 10^{14}$ W/m^2. Simulations show that the experiment[13] was performed below the saturation threshold of the S_1-S_n, T_1-T_2, and $S_0-S_1-T_1$ transitions. It is worthwhile to note that the saturation of the last transition is very sensitive to the values of the Γ_{T_1} and γ_{is} rate constants. One starts to observe the saturation effects ($\rho_{S_1} \approx \rho_{S_n}$ and $\rho_{T_1} \approx \rho_{T_2}$) only for $I > 10^{15}$ W/m^2.

IV. Discussion of Results

Let us first analyze the population dynamics of the singlet and triplet states (Figures 4and 5) for the irradiance $I = 6 \times 10^{14}$ W/m^2. This dynamics have essentially a double-exponential nature with short τ_{ST} (eq 14) and long τ_B (eqs 20 and 21) times. The equilibrium between the S_0 and the T_1 levels is settled during τ_{ST}: ρ_{S_0} decreases from 1 to q in contrast to ρ_{T_1}, which increases from 0 to p (see inset in Figure 5); later on all levels

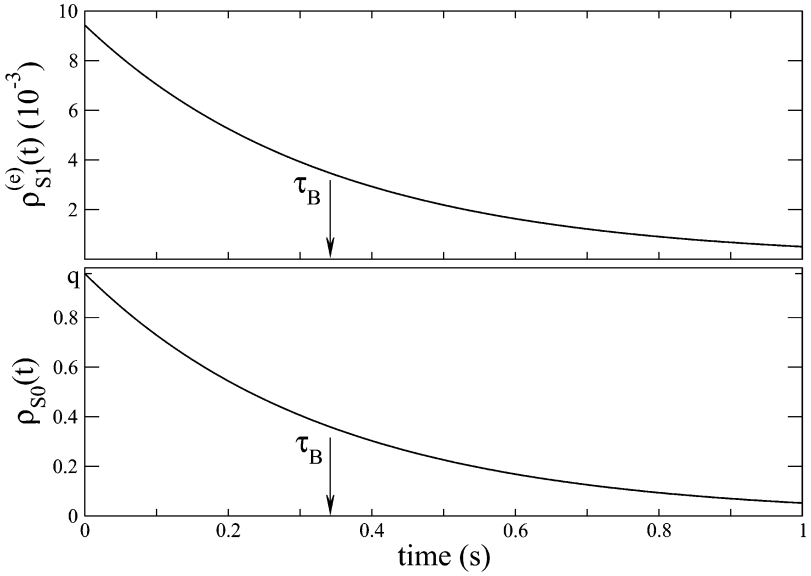

Figure 4. Dynamics of population of the ground state S_0 (lower panel) and envelope of population ρ_{S_1} (Figure 3) of the first excited singlet state S_1 (upper panel). Long-term dynamics of ρ_{S_0} are defined by the time of photobleaching τ_B (eq 25). The peak intensity is $I = 6 \times 10^{14}$ W/m^2, $q \approx 0.9769$, and $\tau_B \approx 0.342$ s.

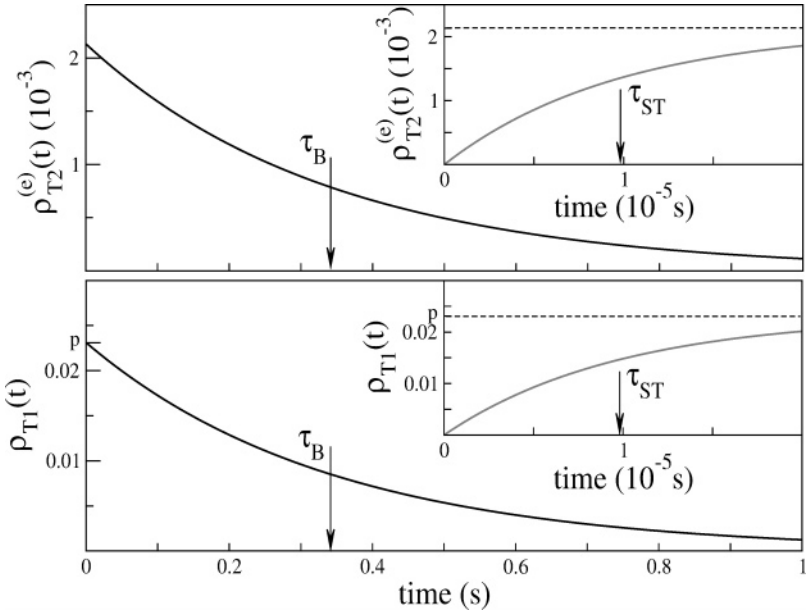

Figure 5. Dynamics of population of the lowest triplet state T_1 (lower panel). Similar to ρ_{S_0} it is of double-exponential character. The T_1 level is populated during $t \lesssim \tau_{ST}$ and starts to depopulate later on when $t \gtrsim \tau_B$. The envelope of population ρ_{T_2} (Figure 3) of the excited triplet state T_2 (upper panel) has dynamics like the one for T_1. Parameters are the same as those in Figure 4, $p \approx 2.31 \times 10^{-2}$, and $\tau_{ST} \approx 9.76 \times 10^{-6}$ s.

are depopulated during τ_B because of the photobleaching (Figure 6). One can see the following relation between the populations, $\rho^{(e)}_{S_1}$, $\rho_{T_1} \ll \rho_{S_0}$. When the intensity grows the concentration of photobleached molecules increases from 0 up to 1 (Figure 6). When the intensity is low $\rho_B \approx t/\tau_B \sim I^2$. The reason for this quadratic law is that the photobleaching from the T_1 and S_1 states dominates.

The effective cross-section σ_3^{eff} (eq 33) of the stepwise three-photon absorption depends weakly on the intensity (Figure 7). The slight decrease of σ_3^{eff} is due to the weak intensity dependence of the effective rate of depopulation $\tilde{\Gamma}_{T_1}$ of the T_1 level (eq 11). The stepwise three-photon absorption influences the effective cross-section of nonlinear absorption $\sigma(I)$ (eq 35), which exceeds significantly the two-photon absorption σ_2 (Figure 7).

The two characteristic times of the photobleaching τ_{ST} and τ_B depend differently on the intensity. Contrary to τ_{ST} (Figure 8A) the photobleaching time τ_B (Figure 8B) decreases strongly when the irradiance is growing (see section IVB).

A. Number of Fluorescence Bursts. The photobleaching decreases the number of intact molecules due to the increase of $\rho_b(t)$. Thus the photobleaching is not a desirable effect in fluorescence microscopy. Indeed, the fluorescence from the first excited state S_1 is proportional to the population of this state (eqs 8 and 24)

$$\rho^{(e)}_{S_1}(t) \approx \gamma\tau(q\ e^{-t/\tau_B} + p\ e^{-t/\tau_{ST}}) \quad \tau_{ST} \ll \tau_B \qquad (37)$$

which displays a double-exponential decay. Here $\rho^{(e)}_{S_1}(t)$ is the envelope of $\rho_{S_1}(t)$ (Figure 4). Let us compute the number of

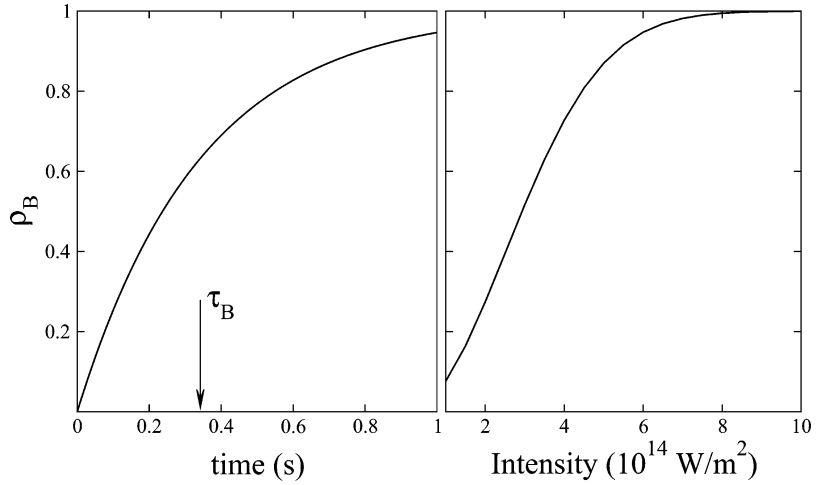

Figure 6. Concentration of photobleached molecules increasing when the irradiance time increases according to eq 24: parameters are the same as those in Figure 4 (left graph; when the peak intensity grows (here irradiance time $t = 1$ s) (right graph).

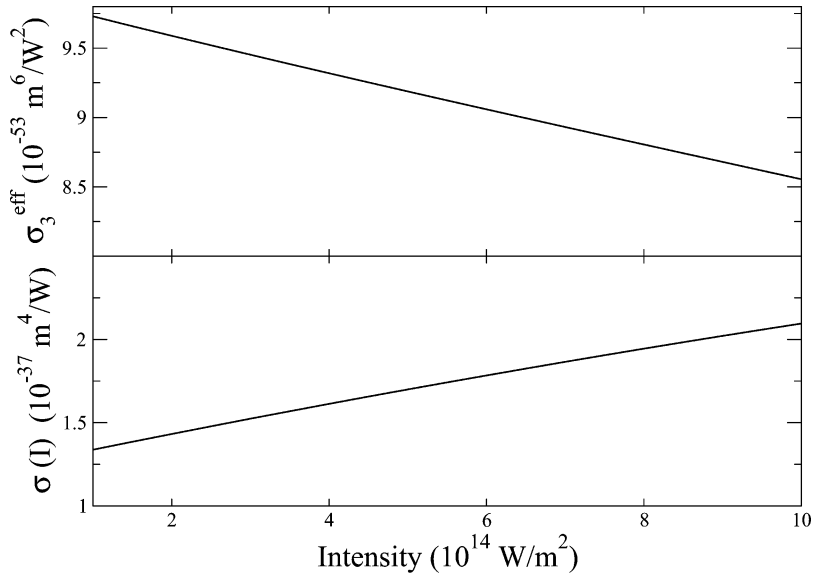

Figure 7. Effective three-photon absorption cross-section (eq 33) (upper panel) and total cross-section of nonlinear absorption (eq 35) (lower panel) versus peak intensity.

fluorescence bursts $n_f(t)$ induced by the nth pulse $t \approx n\Delta$ using the rate equation

$$\frac{\partial n_f(t)}{\partial t} = \Gamma^r_{S_1}\rho_{S_1}(t) \tag{38}$$

Here $\Gamma^r_{S_1}$ is the rate of radiative decay of the S_1 state, which usually gives the dominant contribution to $\Gamma_{S_1} = \Gamma^r_{S_1} + \Gamma^{nr}_{S_1}$, where $\Gamma^{nr}_{S_1}$ is the rate of nonradiative decay or the rate of internal conversion. Integration of this equation from $n\Delta + \tau$ until $n\Delta + \Delta$ (neglecting fluorescence during the pulse) is straightforward using $\rho_{S_1}(t) = \rho^{(e)}_{S_1}(t)\exp(-(\Gamma_{S_1} + \gamma_{is} + k_{S_1})t)$

$$n_f(t) \approx \phi_f\rho^{(e)}_{S_1}(t) = \phi_f\gamma\tau(q\,e^{-t/\tau_B} + p\,e^{-t/\tau_{ST}})$$
$$\Delta \gg (\Gamma_{S_1} + \gamma_{is} + k_{S_1})^{-1} \tag{39}$$

The fluorescence yield

$$\phi_f = \frac{\Gamma^r_{S_1}}{\Gamma_{S_1} + \gamma_{is} + k_{S_1}} \tag{40}$$

varies in the interval $\phi_f = 0.22-0.76$ for molecules studied in ref 9. We would like to pay attention to the fact that the number of fluorescence bursts $n_f(t)$ decays double-exponentially in contrast with the concentration of photobleached molecules $\rho_B(t)$ (eq 24). To obtain the total number of the fluorescence bursts $N_f(t)$ and fluorescence brightness[11] $\beta(t)$ we have to sum all pulses until t $N_f(t) = \sum n_f(n\Delta)$

$$N_f(t) = N_f(\infty)[\zeta(1 - e^{-t/\tau_B}) + (1 - \zeta)(1 - e^{-t/\tau_{ST}})] \quad \beta(t) = \frac{N_f(t)}{t} \tag{41}$$

where

$$N_f(\infty) = \phi_f\gamma(q\tau_B + p\tau_{ST})\frac{\tau}{\Delta} \quad \zeta = \frac{q\tau_B}{q\tau_B + p\tau_{ST}} \tag{42}$$

We are now at the stage to discuss the earlier observed[3,13] double-exponential decay of the fluorescence. The physics of this effect have been unclear. The double-exponential law given by eq 39 cannot explain the experiment[13] due to the small value of $p \ll 1$ and because of the too short time $\tau_{ST} \lesssim 10^{-5}$ s.

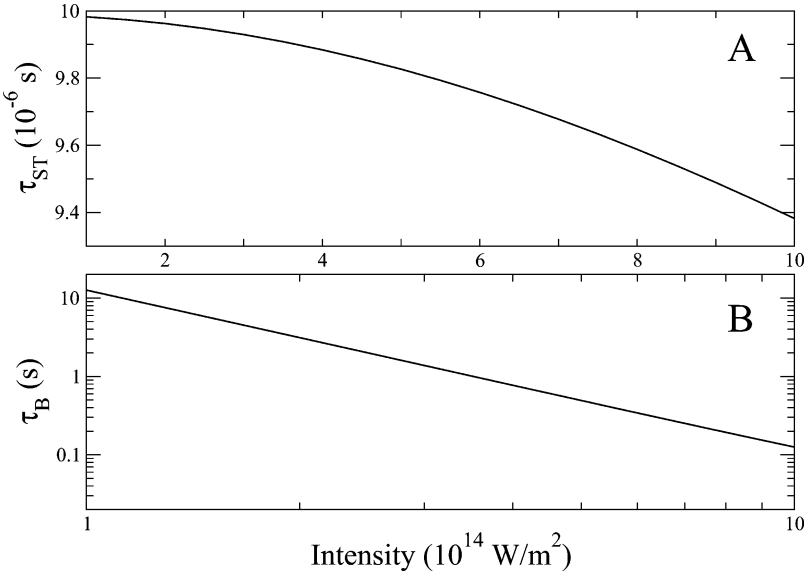

Figure 8. (A) Time of settling of ST equilibrium (eq 14) becomes shorter for larger intensity *I*. (B) The log−log plot shows a quadratic dependence of the photobleaching time (eq 25) on the peak intensity.

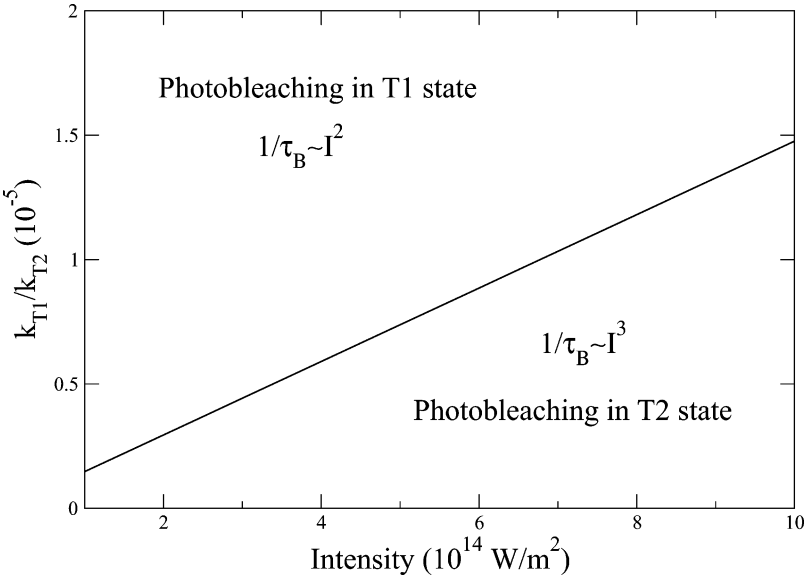

Figure 9. Solid line divides the plane into two regions (eq 46). The photobleaching from the T_1 and S_1 levels dominates in the upper region, while the lower region corresponds to photobleaching mostly occurring in the higher excited states T_2 and S_n.

However, there is another reason for the double-exponential decay, namely, the intensity dependence of the photobleaching rate and the spatial inhomogeneity of the illumination.[28,29] The spatial distribution of the light pulse is not homogeneous due to two reasons. The first one is the attenuation of irradiance due to absorption; the second reason refers to the Gaussian distribution of the light

$$I(r) = I(0)\, \mathrm{e}^{-r^2/a^2} \tag{43}$$

where a is the radius of the light beam. Due to this transverse inhomogeneity the illuminated region can approximately be divided in two parts. The first one is the focal region with high intensity and hence large photobleaching rate $1/\tau_{B1}$. However, the photobleaching rate is significantly smaller ($1/\tau_{B2}$) in the outermost low-intensity region (Figure 10). Thus the inhomogeneity of the light beam leads to a breakdown of the single-exponential decay of fluorescence and photobleaching. To analyze strictly the role of beam inhomogeneity we have to integrate n_f (eq 39) over the whole light beam. The photobleaching rate (see section IVB) depends quadratically on the intensity $1/\tau_B(r) = 1/\tau_B(0)\, \exp(-2r^2/a^2)$ as well as the prefactor $\gamma q \approx \gamma \propto I^2(r)$ in eq 39. This allows us to obtain an analytical expression for the fluorescence integrated over the full cross-section of the light beam

$$\bar{n}_f(t) = 2\pi \int_0^\infty n_f(t) r\, \mathrm{d}r = \frac{\pi}{2}\, \phi_f \tau \gamma(0) a^2\, \frac{1 - \exp(-t/\tau_B(0))}{t/\tau_B(0)} \tag{44}$$

where $\gamma(0) = \gamma(r = 0)$. One can see that the long time asymptotic limit is not exponential, $\bar{n}_f(t) \approx$ constant/t. However, the simulations indicate that the fluorescence can be fitted nicely by a double-exponential function

$$\bar{n}_f(t) \approx A_1\, \mathrm{e}^{-k_1 t} + A_2\, \mathrm{e}^{-k_2 t} \quad t < T \tag{45}$$

when the time of observation T is restricted. The fitting parameters A_1, k_1, A_2, and k_2 depend on T. We use $T = 30$ s as in the experiment.[13] The results of simulations based on the

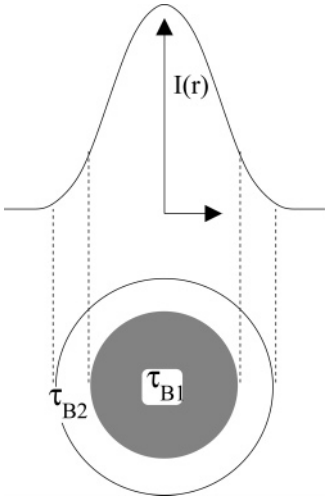

Figure 10. Double-exponential photobleaching caused by the inhomogeneous transverse distribution of the light pulse: $\tau_{B1} < \tau_{B2}$.

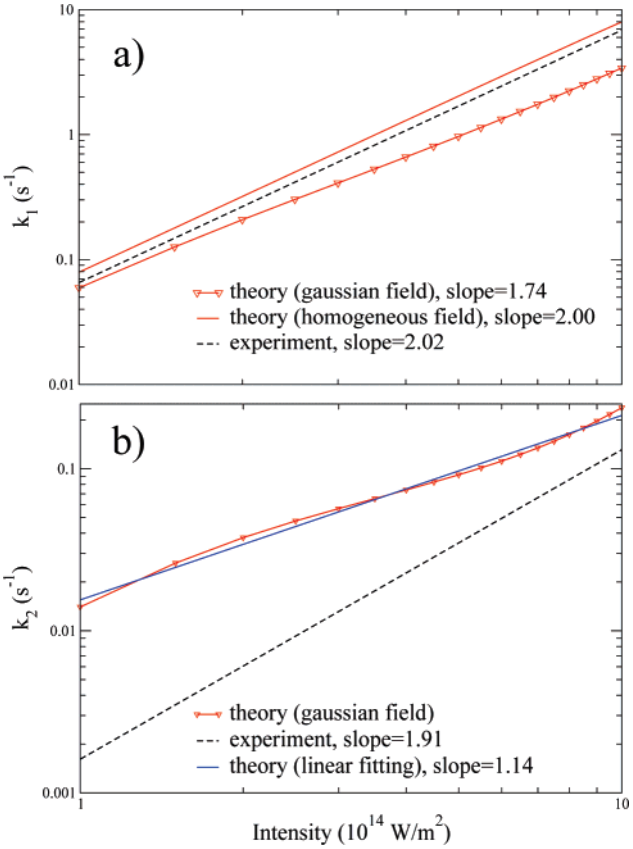

Figure 11. Rates of the photobleaching (a) k_1 and (b) k_2. Triangles mark k_1 and k_2 calculated for a Gaussian beam using the double-exponential fitting (eq 45). The experimental data of Polyzos et al.[13] based on the double-exponential fitting (eq 45) are shown by the dashed line. (a) The solid line shows the photobleaching rate $k_1 = 1/\tau_B$ calculated for a homogeneous light beam (eq 25). (b) The solid line is drawn through the theoretical curve to display the slope.

fitting of the double-exponential expression (eq 45) are shown in Figure 11. We used in the simulation the half width at half-maximum (HWHM) of the Gaussian beam $a_{HWHM} = 0.5\ \mu m$ ($a = a_{HWHM}/\sqrt{\ln 2}$). The theoretical results are in reasonable agreement with experiment[13] for k_1. The agreement is though worse for the slower rate k_2, which mimics the slow power-law decay (t^{-1}) by the exponential function, $\exp(-k_2 t)$.

We computed also the intensity dependencies of k_1 and k_2 for the top-hat beam, which we mimicked by the Gaussian (eq 43) cut at $r = R$. We have found that the slope of $k_2(I)$ is more sensitive to R than $k_1(I)$. For the slope of k_2 we obtained the value close to the experimental one for $R = a$. We also obtain a rather close agreement with the experiment (Figure 12) for the ratio A_1/A_2 of the "fast" and "slow" contributions (eq 45).

In general, it is can be recommended to experimentalists to use the formula in eq 44 instead of the double-exponential formula (eq 45).

It is important to mention that in the case of solutions the double-exponential kinetics can be caused also by an absorption of the dye to the cell surface.[3]

B. Competition between Photobleaching from the T_1, S_1, T_2, and S_n, States. Let us try to shed light on the role of the photobleaching in different excited states. According to our model (see section IIIB and Table 2), $k_{T_1} = k_{S_1} = 107\ s^{-1}$ and $k_{T_2} = k_{S_n} = 10^6\ s^{-1}$. The simulations (Figures 4 and 5) show that the population of the S_1 level is comparable with the population of T_1 during the interaction with the pulse ($\tau = 100$ fs). The first impression is that contributions of these two levels for the total rate of photobleaching are comparable. However, this is actually not the case because we have to take into account also the photobleaching that occurs between pulses during $\Delta \approx 12$ ns. The photobleaching in the long-lived T_1 state dominates here because of the fast depopulation of the S_1 level during $\Gamma_{S_1}^{-1} = 3$ ns. This means that the overall photobleaching in the T_1 state is noticeably larger than that in the S_1 state, because $\Delta \gg \tau$. Finally, the total photobleaching rate is affected by competition between photobleaching in the T_1, S_1, and (T_2 or S_n) states with quadratic and cubic intensity dependences, respectively.

In the studied region of peak intensities I, the relaxation rate Γ_{T_1} gives a dominant contribution in the denominator of the expression for the bleaching time (eq 25). This allows us to understand the intensity dependence of the photobleaching bearing in mind that the rate of the two-photon transition S_0-S_1 depends quadratically on intensity ($\gamma \propto I^2$) contrary to the one-photon transitions S_1-S_n or T_1-T_2 (γ_T, $\gamma_S \propto I$). We assumed for the numerical simulations that $k_{S_1} = k_{T_1}$, $k_{S_n} = k_{T_2}$, and $\Gamma_{S_1} \gg k_{S_1} + \gamma_{is}$, $\Gamma_{S_n} = \Gamma_{T_2} \gg k_{S_n}$, k_{T_2} (see section IIIB). Taking this into account and collecting terms with quadratic and cubic intensity dependences in the equation for $1/\tau_B$ (eq 25) one can obtain the following equation for the interface between the quadratic and the cubic laws for the photobleaching rate $1/\tau_B$: (Figure 9)

$$\frac{k_{T_1}}{k_{T_2}} = \frac{(2\gamma_{is}\gamma_T + \Gamma_{T_1}\gamma_S\Gamma_{S_1}\Delta)}{2\Gamma_{T_2}(\gamma_{is} + \Gamma_{T_1})}\frac{\tau}{\Delta} \qquad (46)$$

The results of the simulations shown in Figure 11 display a quadratic dependence of the rate of the "fast" photobleaching with $k_{T_1}/k_{T_2} = 1.07 \times 10^{-4}$ in agreement with Figure 9.

C. Different Regimes of Photobleaching. Experiment[13] shows a cubic intensity dependence of the photobleaching rate for the pyrylium salts C2, C3, and C4 (Figure 1a). To obtain such a cubic dependence we need a smaller ratio of k_{T_1}/k_{T_2}, namely, $k_{T_1}/k_{T_2} < 0.8 \times 10^{-5}$ for $I = 6 \times 10^{14}$ W/m ^{2}. Cubic dependence means that the photobleaching mostly occurs in the T_2 and S_n states. However, according to Figure 9, this happens when the intensity is high (central part of the light beam, Figure 10). It is not hard to understand that for the T_1 state the photobleaching occurs in the wings of the light beam where the intensity is not sufficiently high to significantly populate the T_2 and S_n states. This case indicates that the double-exponential decay (eq 45) observed for the pyrylium salts C2,

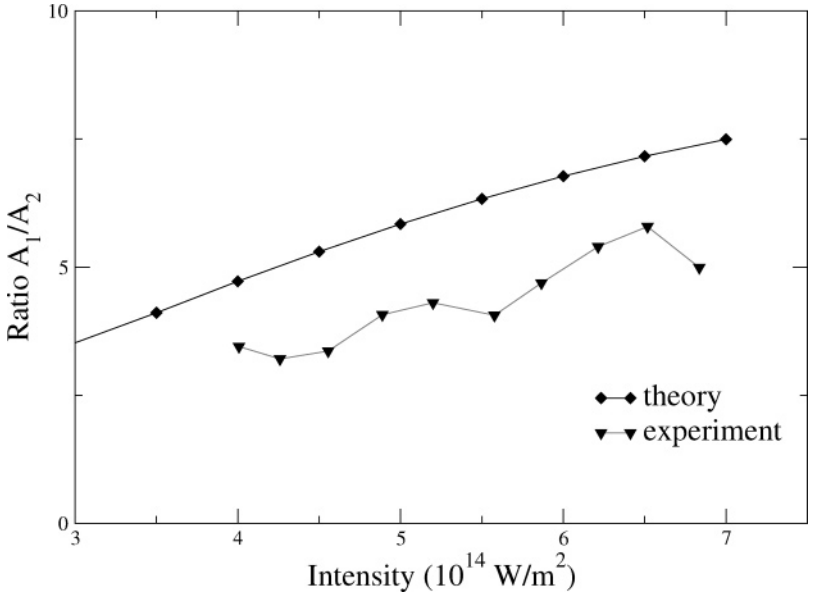

Figure 12. Comparison of theoretical and experimental[13] ratio A_1/A_2 of "fast" and "slow" contributions A_1/A_2 (eq 45).

C3, and C4 is related also to the different photochemistry in different parts of the light beam: fast photobleaching in the T_2 and S_n states in the central part of the beam and slow photobleaching in the T_1 state at the wings of the beam.

D. Role of Saturation. As already mentioned, the saturation of spectral transitions is negligible in the studied region of intensities. However, simulations show that saturation becomes important when the irradiance exceeds $I = 10^{15}$ W/m^2. The saturation of the $S_0-S_1-T_1$ transition is taken into account by the term $\gamma\phi_{isc}$ in the denominator of the expression for p (eq 13). Saturation of the one-photon transition $T_1 \rightarrow T_2$ is taken into account using the following replacement[30]

$$\gamma_T\tau \rightarrow \frac{\kappa[1-\exp(-\tau\bar{\Gamma}_{T_2}(1+\kappa))]}{2(1+\kappa)} \quad \kappa = \frac{2\gamma_T}{\bar{\Gamma}_{T_2}} \qquad (47)$$

where $\bar{\Gamma}_{T_2} = \Gamma_{T_2} + k_{T_2}$. A similar replacement is used for the $S_1 \rightarrow S_n$ transition.

V. Summary

Photochemical reactions remove molecules from the absorption−emission cycle. Due to this circumstance photobleaching becomes important in fluorescence imaging as well as in read−write processes used for three-dimensional optical data storage. We have in this article presented a dynamical theory of multiphoton-induced fluorescence accompanied by photobleaching. Our model includes a manifold of singlet and triplet states. The lowest triplet state has a permanent population due to the long lifetime, meaning that the photobleaching occurs mostly from this state and that a quadratic dependence of characteristic bleaching time on light intensity is observed.

We obtain simple analytical expressions for the main characteristics of fluorescence accompanied by photobleaching, namely, the photobleaching time. This time depends on the peak intensity, repetition rate, pulse duration, and microscopic parameters of the single molecule such as the absorption cross-section, relaxation rates, and rate of intersystem crossing. We carried out first-principles simulations to obtain the cross-sections of nonlinear absorption and resonant frequencies for the pyrylium salt 4-methoxyphenyl-2,6-bis(4-methoxyphenyl) pyrylium tetrafluorobate used for numerical illustration. The presented theory explains recent experimental results of Polyzos et al.,[13] which display either quadratic or cubic intensity dependence of the photobleaching time for different pyrylium salts.

We suggest two qualitatively different mechanisms of the observed double-exponential dynamics of laser-induced fluorescence. The first one gives two characteristic times of the fluorescence decay: the equilibrium settling time between the ground and the lowest triplet states and the duration of photobleaching. However, the first time is too short to explain the experiment in ref 13. Our simulations show that the spatial inhomogeneity of the light beam, which constitutes the ground state of the second mechanism, is the main reason for the observed double-exponential law. We find that the microscopic mechanism of photobleaching in the general case can be different in the beam center (high intensity) and in the beam tail (low intensity) due to the low population of higher excited states at the wings of the beam. The numerical simulations show that the cross-section of nonlinear absorption deviates significantly from two-photon absorption due to the stepwise absorption from the first excited singlet and triplet states.

Appendix A: Derivation of Eq 9

It is convenient to rewrite eq 1 for ρ_{T_1} as follows

$$\frac{\partial}{\partial t}\rho_{T_1} = \gamma_{is}\rho_{S_1} - (\Gamma_{T_1} + k_{T_1})\rho_{T_1} - Q(t)$$

$$Q(t) = \frac{\partial}{\partial t}\rho_{T_2} + k_{T_2}\rho_{T_2} \qquad (A1)$$

The term $Q(t)$ describes the one-photon transfer of the population between the T_1 and the T_2 levels accompanied by the photobleaching from the T_2 state. We note that this term can be ignored when $k_{T_2} = 0$ because $Q(t)$ gives small and fast fluctuation of the T_1 population during the $\tau + 1/\Gamma_{T_2}$ interval, which does not affect the average population of this level. However, the photobleaching in the T_2 state gives a slow depopulation of the lowest triplet state. Because this slow

depopulation is important only at a large time scale it is natural to treat the $Q(t)$ term at the average

$$Q(t) \rightarrow \overline{Q(t)} = \frac{1}{\Delta}\int_{n\Delta}^{(n+1)\Delta} Q(t)\,\mathrm{d}t \approx \frac{k_{T_2}}{\Delta}\int_{n\Delta}^{(n+1)\Delta} \rho_{T_2}(t)\,\mathrm{d}t \quad \text{(A2)}$$

Here we use the fact that the level T_2 is depopulated during the time interval between pulses: ${\rho_{T_2}}^n \approx {\rho_{T_2}}^{n+1} \approx 0$. The reason for this is found in the fast relaxation of the T_2 state in comparison with spacing between pulses $\Gamma_{T_2}^{-1} \ll \Delta$. Equation A2 indicates that the large scale dynamics of the population exchange between the T_1 and the T_2 levels is affected only by the quenching of $\rho_{T_1}(t)$ caused by the photobleaching. Making use of this approximation we ignore the short-lived deviation of ρ_{T_1} from the envelope (Figure 3) caused by population exchange between the triplet states. To find $\overline{Q(t)}$ we need the solution of eq 1 for ρ_{T_2} during the nth pulse $\rho_{T_2}^{(I)}$ and between the nth and $(n+1)$th pulses $\rho_{T_2}^{(II)}$

$$\rho_{T_2}^{(I)}(t) = \frac{{\rho_{T_1}}^n \gamma_T}{\Gamma_{T_2} + k_{T_2} + 2\gamma_T}(1 - \exp(-(\Gamma_{T_2} + k_{T_2} + 2\gamma_T)(t - n\Delta))) \quad n\Delta \le t \le n\Delta + \tau$$

$$\rho_{T_2}^{(II)}(t) = \rho_{T_2}^{(I)}(n\Delta + \tau)\exp[-(\Gamma_{T_2} + k_{T_2})(t - (n\Delta + \tau))] \quad n\Delta + \tau \le t \le (n+1)\Delta \quad \text{(A3)}$$

Integration of this solution over time gives

$$\frac{\partial}{\partial t}\rho_{T_1} \approx \gamma_{is}\rho_{S_1} - \left(\Gamma_{T_1} + k_{T_1} + \frac{\alpha}{\Delta}\right)\rho_{T_1} \quad \text{(A4)}$$

The fraction of bleached molecules α (eq 11) in the T_2 state (relative to the concentration of molecules in the T_1 state) per pulse is a product of the fraction of the molecules in the T_2 state ($\gamma_T\tau$) and the branching ratio of photobleaching from the T_2 state $æ_{T_2}$ (eq 11). It is relevant to note that $\alpha \ll 1$ due to eq 5.

Let us write eq 1 for the S_0, S_1, and T_1 levels for the time $t \in (n\Delta + \tau, n\Delta + \Delta)$ between the nth and $(n+1)$th pulses where $\gamma(t) = 0$

$$\frac{\partial}{\partial t}\rho_{S_0} = \Gamma_{S_1}\rho_{S_1} + \Gamma_{T_1}\rho_{T_1}$$

$$\frac{\partial}{\partial t}\rho_{S_1} = -(\Gamma_{S_1} + \gamma_{is} + k_{S_1})\rho_{S_1} + \Gamma_{S_n}\rho_{S_n}$$

$$\frac{\partial}{\partial t}\rho_{T_1} = \gamma_{is}\rho_{S_1} - \left(\Gamma_{T_1} + k_{T_1} + \frac{\alpha}{\Delta}\right)\rho_{T_1} \quad \text{(A5)}$$

Let us solve eq A5 taking into account the particle conservation law (eq 7) and neglecting the short-lived term $\Gamma_{S_n}\rho_{S_n}$. From the second eq A5 we obtain

$$\rho_{S_1}(t - n\Delta - \tau) = \gamma\tau{\rho_{S_0}}^n \exp(-(\Gamma_{S_1} + \gamma_{is} + k_{S_1})(t - n\Delta - \tau)) \quad \text{(A6)}$$

Integration of the third equation in eq A5 with this expression for ρ_{S_1} gives

$$\rho_{T_1}(t - n\Delta - \tau) = -\phi_{isc}\gamma\tau{\rho_{S_0}}^n \exp(-(\Gamma_{S_1} + \gamma_{is} + k_{S_1})(t - n\Delta - \tau)) + ({\rho_{T_1}}^n + \phi_{isc}\gamma\tau{\rho_{S_0}}^n)\exp(-\tilde{\Gamma}_{T_1}(t - n\Delta - \tau)) \quad \text{(A7)}$$

where ϕ_{isc} and $\tilde{\Gamma}_{T_1}$ are defined by eqs 10 and 11 accordingly. The concentration of the ground-state molecules ρ_{S_0} before the $n+1$ pulse is found directly from eq 7. Now we are at the stage to write down the populations ρ^{n+1} just before the $(n+1)$ pulse ($t = (n+1)\Delta$)

$${\rho_{S_0}}^{n+1} = 1 - {\rho_b}^{n+1} - ({\rho_{T_1}}^n + \phi_{isc}\gamma\tau{\rho_{S_0}}^n)\exp(-\tilde{\Gamma}_{T_1}\Delta)$$

$${\rho_{S_1}}^{n+1} = \gamma\tau{\rho_{S_0}}^n \exp(-(\Gamma_{S_1} + \gamma_{is} + k_{S_1})\Delta) \ll {\rho_{S_0}}^n$$

$${\rho_{T_1}}^{n+1} = ({\rho_{T_1}}^n + \phi_{isc}\gamma\tau{\rho_{S_0}}^n)\exp(-\tilde{\Gamma}_{T_1}\Delta) \quad \text{(A8)}$$

The contributions $\propto {\rho_{S_1}}^n$ are neglected in the expressions for ${\rho_{S_0}}^{n+1}$ and ${\rho_{T_1}}^{n+1}$ because $\exp(-(\Gamma_{S_1} + \gamma_{is} + k_{S_1})\Delta) \ll 1$. We have already used this implicitly in eq 8 assuming $\rho_{S_1}(n\Delta - 0) = 0$ just before a pulse. The first equation in eq A8 results immediately in eq 9 when we use ${\rho_{T_1}}^n \approx 1 - {\rho_b}^n - {\rho_{S_0}}^n$, and take into account that $\rho_b(t)$ depends much slower on the time compared with $\rho_{S_0}(t)$

$${\rho_b}^{n+1} \approx {\rho_b}^n \quad \text{(A9)}$$

due to $\tau_{ST} \ll \tau_B$.

Acknowledgment. We thank Professor Peter Persephonis for valuable discussions. The authors acknowledge support from the Swedish Research Council, the STINT foundation, and a grant from the photonics project, run jointly by the Swedish Material Administration and the Swedish Defense Research Agency.

References and Notes

(1) Petersson, G. H.; Piston, D. W. *Biophys. J.* **2000**, *78*, 2159.
(2) Eggeling, C.; Volkmer, A.; Seidel, C. A. M. *ChemPhysChem* **2005**, *6*, 791.
(3) Eggeling, C.; Widengren, J.; Rigler, R.; Seidel, C. A. M. *Anal. Chem.* **1998**, *70*, 2651.
(4) Mertz, J. *Eur. Phys. J. D* **1998**, *3*, 53.
(5) Deschenes, L. A.; Vanden Bout, D. A. *Chem. Phys. Lett.* **2002**, *365*, 387.
(6) Gu, M.; Day, D. *Opt. Lett.* **1999**, *24*, 287.
(7) Polyzos, I.; Tsigaridas, G.; Fakis, M.; Giannetas, V.; Persephonis, P. *Opt. Lett.* **2005**, *30*, 2654.
(8) Parthenopoulos, D. A.; Rentzepis, P. M. *Science* **1989**, *245*, 843.
(9) Polyzos, I.; Tsigaridas, G.; Fakis, M.; Giannetas, V.; Persephonis, P.; Mikroyannidis, J. *Chem. Phys. Lett.* **2003**, *369*, 264.
(10) Prasad, P. N. *Introduction to Biophotonics*; Wiley-Interscience: Hoboken, NY, 2003.
(11) Eggeling, C.; Widengren, J.; Brand, L.; Schaffer, J.; Felekyan, S.; Seidel, C. A. M. *J. Phys. Chem. A* **2006**, *110*, 2979.
(12) Donnert, G.; Eggeling, C.; Hell, S. W. *Nat. Methods* **2007**, *4*, 81.
(13) Polyzos, I.; Tsigaridas, G.; Fakis, M.; Giannetas, V.; Persephonis, P.; Mikroyannidis, J. *J. Phys. Chem. B* **2006**, *110*, 2593.
(14) Polyutov, S.; Minkov, I.; Gel'mukhanov, F.; Ågren, H. *J. Phys. Chem. A* **2005**, *109*, 9507.
(15) (a) Becke, A. D. *J. Chem. Phys.* **1993**, *98*, 5684. (b) Lee, C.; Yang, W.; Parr, R. G. *Phys. Rev. B* **1988**, *37*, 785.
(16) (a) Ditchfield, R.; Hehre, W. J.; Pople, J. A. *J. Chem. Phys.* **1971**, *54*, 724. (b) Hehre, W. J.; Ditchfield, R.; Pople, J. A. *J. Chem. Phys.* **1972**, *56*, 2257.
(17) Sałek, P.; Vahtras, O.; Helgaker, T.; Ågren, H. *J. Chem. Phys.* **2002**, *117*, 9630.
(18) Tunell, I.; Rinkevicius, Z.; Vahtras, O.; Sałek, P.; Helgaker, T.; Ågren, H. *J. Chem. Phys.* **2003**, *119*, 11024.
(19) (a) Furche, F. *J. Chem. Phys.* **2001**, *114*, 5982. (b) Salek, P.; Vahtras, O.; Helgaker, T.; Ågren, H. *Chem. Phys. Lett.* **2003**, *374*, 446.
(20) Jha, P. C.; Luo, Y.; Polyzos, I.; Persephonis, P.; Ågren, H. *Chem. Phys. Lett.*, in press.
(21) Baev, A.; Gel'mukhanov, F.; Macak, P.; Luo, Y.; Ågren, H. *J. Chem. Phys.* **2002**, *117*, 6214.
(22) Tripathi, S.; Wintgens, V.; Valat, P.; Toscano, V.; Kossannyi, J. *J. Lumin.* **1987**, *37*, 149.

(23) Baunsgaard, D.; Larsen, M.; Harrit, N.; Frederiksen, J.; Wilbrandt, R.; Stapelfeldt, H. *J. Chem. Soc., Faraday Trans.* **1997**, *93*, 1893.
(24) Akaba, R.; Kamata, M.; Koike, A.; Mogi, K.-I.; Kuriyama, Y.; Sakuragi, H. *J. Phys. Org. Chem.* **1997**, *10*, 861.
(25) Álvaro, M.; Aprile, C.; Carbonell, E.; Ferrer, B.; García, H. *Eur. J. Org. Chem.* **2006**, *11*, 2644.
(26) Müller, C.; Wasserberg, D.; Weemers, J. J. M.; Pidko, E. A.; Hoffmann, S.; Lutz, M.; Spek, A. L.; Meskers, S. C. J.; Janssen, R. A. J.; van Santen, R. A.; Vogt, D. *Chem.—Eur. J.* **2007**, *13*, 4548.
(27) Tsien, R. Y.; Ernst, L.; Waggoner, A. Fluorophores for confocal microscopy: Photophysics and photochemistry. In *Handbook of Biological Confocal Microscopy*, 3rd ed.; Pawley, J. B., Ed.; Springer: New York, 2006; pp 338−352.
(28) Widengren, J.; Mets, Ü.; Rigler, R. *J. Phys. Chem.* **1995**, *99*, 13368.
(29) Prummer, M.; Weiss, M. *Phys. Rev. E* **2006**, *74*, 021115.
(30) Gel'mukhanov, F.; Baev, A.; Macak, P.; Luo, Y.; Ågren, H. *J. Opt. Soc. Am. B* **2002**, *19*, 937.